d- and *sp*-like surface states on fcc Co(001) with distinct sensitivity to surface roughness

T. Allmers* and M. Donath†

Physikalisches Institut, Westfälische Wilhelms-Universität Münster, Wilhelm-Klemm-Straße 10, 48149 Münster, Germany

J. Braun, J. Minár, and H. Ebert

Department Chemie, Ludwig-Maximilians-Universität München, Butenandtstraße 5-13, 81377 München, Germany

(Received 11 October 2011; revised manuscript received 29 November 2011; published 14 December 2011)

The sensitivity of electronic surface states to modifications of the surface topography has been investigated in regard to the orbital character of the respective states. The surface of face-centered-cubic Co(001) shows two characteristic electronic states: an occupied *d*-like minority surface state around the center of the surface Brillouin zone $\bar{\Gamma}$ and an unoccupied *sp*-like surface state with an exchange splitting of 0.56 eV around the zone boundary $\bar{X}$. These states were studied experimentally on a 15-monolayer Co film on Cu(001) by spin-resolved direct and inverse photoemission. In addition, the Co(001) surface was theoretically described by calculations of the Bloch spectral function and of the direct and inverse photoemission intensities within the one-step-model approach. Different surface topographies from atomically smooth to very rough, as proved by scanning tunneling microscopy, were achieved by choosing varied growth and annealing temperatures for the preparation of the Co films. Both types of surface states are highly sensitive to the film roughness, yet in a distinctly different way. The less localized *sp*-like wave function causes a much higher sensitivity of the unoccupied surface state to lateral inhomogeneities than the more localized *d*-type wave function of the occupied surface state.

DOI: 10.1103/PhysRevB.84.245426 PACS number(s): 73.20.−r, 68.55.J−, 75.50.Cc, 79.60.−i

I. INTRODUCTION

Defect scattering at surfaces and interfaces play an important role for interface phenomena, e.g., the giant magnetoresistance effect, as well as for transport properties relevant for device applications. Therefore they are studied in detail to date. Defect scattering and disorder-dependent dephasing processes were investigated by high-resolution photoemission on rough Cu(111) surfaces.[1] The scattering of hot electrons by adatoms at metal surfaces was the subject of a time-resolved two-photon-photoemission study of Cu adatoms on Cu(001).[2] Two-dimensional electron transport through surface states in Bi(111) was shown to be strongly dependent on surface roughness.[3] Controlling surface or interface roughness during device fabrication is by no means a trivial task. Furthermore, the sensitivity of electronic surface states to roughness depends on the character of their wave functions.

The preparation of ultrathin face-centered-cubic (fcc) Co films in Cu(001) has been refined since the early days of thin-film growth. The morphology (i.e., the film topography and its chemical composition) of ultrathin Co films is influenced by minor variations in the growth conditions (see Ref. 4 and references therein). In particular, we have recently shown in a scanning tunneling microscopy (STM) study that the morphology of Co films on Cu(001) can be tailored by varying the preparation conditions.[4] In addition, *d*- and *sp*-derived surface states have been detected and expected, respectively, on this surface. It may therefore serve as a suitable test case for studying the sensitivity of surface states on roughness in regard to their orbital character.

In this contribution, we focus on 15-ML (monolayer)-thick Co films on Cu(001), which are free of Cu impurities from the substrate. As an example for a *d*-like surface state, we investigated a recently detected occupied minority surface state, which appears around the center of the surface Brillouin zone (SBZ) $\bar{\Gamma}$.[5,6] As an example for a *sp*-like surface state, we looked for an unoccupied state, which is expected to appear around the zone boundary $\bar{X}$. This kind of state was detected in former studies on various fcc(001) metal surfaces[7–9] but not for Co(001) so far. We identified this state and determined its magnetic exchange splitting using spin-resolved inverse photoemission. For both surface states, we tested their sensitivity to the film roughness.

Our experimental investigations are accompanied by a theoretical analysis. Due to pronounced correlation effects present in the valence-band spectra of 3*d*-transition metals like Co, which are not well described by plain single-particle approaches like the local-spin-density approximation (LSDA),[10–13] we used a self-consistent combination of the LSDA and the dynamic mean-field theory (DMFT)[14,15] to calculate the electronic structure of in-plane magnetized fcc Co(001).[11,13] A direct link to our spectroscopical experiments is provided by a complete calculation of spectra within the fully relativistic one-step model of photoemission that is based on the LSDA+DMFT electronic structure input and additionally takes care of the surface by a realistic model of the surface potential, which is given by a spin-dependent Rundgren-Malmström barrier.[16] Using this analytical procedure, we were able to achieve a quantitative agreement with the experimental data, although more sophisticated many-body theories are in principle needed due to the presence of nonlocal correlations in ferromagnetic Co.

This paper is organized as follows: The experimental and computational details are described in Secs. II A and II B, respectively. In Sec. III A we present the results for the occupied minority surface state. Experimental and theoretical evidence of the unoccupied spin-split surface state around $\bar{X}$ is given in Sec. III B. These sections contain also experimental results for varying surface roughness. A summary of the results is given in Sec. IV.

II. EXPERIMENTAL AND COMPUTATIONAL DETAILS

A. Experimental details

The experiments were performed in an ultrahigh-vacuum apparatus equipped with multiple techniques for surface preparation and characterization. The base pressure was better than 3×10^{-9} Pa.

The Cu(001) substrate was cleaned by bombardment with Ar^+ ions (1 keV) and subsequently annealed to 850 K. The sputtering and annealing cycles were repeated until no contamination was detected with Auger electron spectroscopy (AES) within the detection limit of 1% to 5% of a monolayer (ML) depending on the impurity. At this point the low-energy electron diffraction (LEED) measurements revealed a sharp (1×1) pattern with low background. Terrace widths of more than 80 nm were found with STM.

Co was evaporated from a high-purity rod by a water-cooled electron-beam evaporator to avoid possible contamination from a crucible. During evaporation the pressure was better than 5×10^{-9} Pa. The evaporation rate was calibrated to $\approx$0.5 ML min^{-1} by recording intensity oscillations of a reflected specular electron beam (medium-energy electron diffraction; see, e.g., Ref. 17).

The spin-dependent electronic structure was characterized using spin- and angle-resolved direct and inverse photoemission (PE and IPE):[18] The PE data were obtained using a 50-mm simulated hemispherical sector analyzer (SHA50 from Focus GmbH). Spin resolution was provided via a spin-polarized low-energy electron diffraction (SPLEED) detector.[19,20] A helium discharge lamp with unpolarized He-I light ($\hbar\omega =$ 21.22 eV) was used for excitation.

The IPE data were retrieved by employing a home-built setup. Electrons from a GaAs photocathode are directed onto the sample with well defined energy (7–14 eV), momentum, and spin.[21,22] The emission of photons is caused by electrons undergoing radiative transitions into lower-lying unoccupied states. Photons are detected at a fixed energy by a Geiger-Müller counter. Its energy selectivity is based on the ionization threshold of acetone used as counting gas and the transmission cutoff of the CaF_2 entrance window. The mean detection energy is $\hbar\omega = (9.9 \pm 0.17)$ eV.[22,23] The counter, used in this study, is placed at angles of about 70° relative to the electron gun in the measurement plane and about 30° out of the measurement plane.

Different sample temperatures during Co deposition (growth temperature T_G) and different annealing temperatures after deposition (annealing temperature T_A) were applied to influence the topography of the Co films. The different preparations are denoted by $\wp(T_G, T_A)$. The resulting topographies were characterized with STM in a detailed growth study published recently.[4] As in this study, we focused on 15-ML-thick Co films in the present work. The different degrees of surface roughness range from very rough (exhibiting only small islands) to atomically smooth surfaces. Despite the different topographies, the long-range crystallographic order is in all cases fcc(001) as revealed by LEED measurements. All surfaces studied here are free from Cu impurities as proved by PE (for details, see Ref. 4).

The spin-resolved PE and IPE measurements were performed after the sample was magnetized in the surface plane along an easy magnetization direction of type ⟨110⟩. For a correct interpretation of the spin-resolved spectra, it is important to know the remanent sample magnetization direction with respect to the spin-polarization direction of the incident electrons. For this reason, we performed magneto-optical Kerr effect measurements for the different Co film preparations studied in this work. In all cases, squarelike hysteresis curves were obtained. The remanent magnetization equals magnetic saturation, which indicates that the sample is remanently magnetized in a one-domain state. Co was evaporated along the surface normal to avoid steering effects.[24] Thus, as expected from the crystalline symmetry, no uniaxial anisotropy was found: Both ⟨110⟩ directions are equivalent magnetization directions. The PE and IPE spectra were measured at sample temperatures of 295 K and below, which corresponds to $T/T_C < 0.2$ (T_C: Curie temperature), i.e., close to the magnetic ground state.

B. Computational details

The self-consistent electronic structure calculations were performed within the *ab initio* framework of spin-density-functional theory. The Vosko, Wilk, and Nusair parametrization of the exchange and correlation potential was used.[25] The electronic structure was calculated in a fully relativistic mode by solving the corresponding Dirac equation. This was achieved using the spin-polarized relativistic multiple-scattering Korringa-Kohn-Rostoker based Munich SPR-KKR program package.[26,27] To account for electronic correlations beyond the LSDA[28,29] we employed a combined LSDA+DMFT scheme, self-consistent in both the self-energy calculation and the charge-density calculation, as implemented within the relativistic SPR-KKR formalism.[30] As a DMFT solver the relativistic version of the so-called spin-polarized T-matrix plus fluctuation exchange (SPTF) approximation[31,32] was used. In contrast to most other LSDA+DMFT implementations, within the SPR-KKR scheme the complex and energy-dependent self-energy Σ_{DMFT} is implemented as an additional energy-dependent potential to the radial Dirac equation, which is solved in order to calculate the new Green's function. This procedure is repeated until self-consistency in both the self-energy and the charge density is achieved. The double counting problem (separation of the Hubbard Hamiltonian from the LSDA one) was considered within the usual around-mean-field (AMF) limit. This scheme was successfully used in describing photoemission from 3*d* transition metals.[10–12]

The self-energy within the DMFT is parametrized by the averaged screened Coulomb interaction U and the Hund exchange interaction J. For Fe, Co, and Ni it is usually accepted that the averaged on-site exchange interaction J coincidences with its atomic value $J \approx 0.9$ eV. This parameter can be calculated directly within the LSDA and is approximately the same for all 3*d* elements.[33] The determination of U is a quite serious problem, and usually semiempirical values are assumed.[34] In fact, the parameter U is strongly affected by the metallic screening and it is estimated for the 3*d* metals between 1 and 3 eV. Here we used $U = 2.2$ eV for Co. With this value for the averaged on-site Coulomb interaction we found the optimal agreement between the experimental and theoretical peak positions.

In our DMFT calculations, we used 4096 Matsubara poles to determine the corresponding SPTF self-energy. The effective potentials were treated within the atomic sphere approximation (ASA). For the multipole expansion of the Green's function, an angular momentum cutoff of $l_{\max} = 3$ was used. The integration in $\boldsymbol{k}$ space was performed by the special points method using 1600 $\boldsymbol{k}$ points in the irreducible wedge.

In our spectroscopical analysis we used the experimentally determined value for the work function $\phi = (4.81 \pm 0.05)$ eV. This value is in accordance with previous results.[35,36] For the photoemission calculations lifetime effects in the initial states have been included via the imaginary part of the complex self-energy obtained from the self-consistent LSDA+DMFT calculation. For the inverse photoemission calculations a heuristic imaginary value $i V_{\mathrm{i}} = 0.05(E - E_{\mathrm{F}})$ was added to $\mathrm{Im}(\Sigma_{\mathrm{DMFT}})$ because of the mostly *sp*-like nature of the unoccupied surface related features, which are located at higher energies. To take care of impurity scattering we used in addition a small constant imaginary value of $i V_{\mathrm{i}} = 0.05$ eV. For the final states a constant imaginary part $i V_{\mathrm{f}} = 1.5$ eV has been chosen, again in a phenomenological way. A realistic description of the surface potential is achieved using a spin-dependent barrier of Rundgren-Malmström type.[16] The parametrization of the Co(001) surface barrier that finally led to a quantitative agreement between the measured and calculated spectra is the following: $z_i^{\uparrow} = -1.93$, $z_i^{\downarrow} = -1.79$, $z_a^{\uparrow,\downarrow} = -3.97$, and $z_e^{\uparrow,\downarrow} = 0.0$. Aside from the fact that the image plane z_i is slightly spin dependent, these barrier parameters are the same ones as used for Cu(001).[37] According to the experimental situation all spectroscopical calculations were performed for an in-plane orientation of the magnetic field, at which the magnetization points parallel to the $\bar{\Gamma}\bar{\mathrm{X}}$ direction (i.e., along $\langle 110 \rangle$) in the corresponding SBZ.

III. RESULTS AND DISCUSSION

A. Occupied *d*-like minority surface state

For fcc Co(001) a *d*-like minority surface state around the $\bar{\Gamma}$ point of the SBZ was identified with spin-resolved PE and two-photon photoemission.[5,6] In accordance with these investigations, our results confirm the surface state $SS_d^{\downarrow}$ at $E - E_{\mathrm{F}} = -0.45$ eV for normal electron emission.

Figure 1 shows our spin-resolved PE results for 15 MLs of Co on Cu(001) prepared under varied conditions. The position of $SS_d^{\downarrow}$ is marked with a gray bar. Pictures of STM measurements on the left-hand side illustrate the corresponding surface topographies.[4] Three different preparations were studied (from bottom to top):

(i) The preparation $\wp(T_{\mathrm{G}} = 115$ K, no annealing) results in a rough surface due to the suppressed mobility of Co adatoms at low growth temperature. The surface exhibits islands with a size between 3 and 6 nm.

(ii) The preparation $\wp(T_{\mathrm{G}} = 295$ K, no annealing) results in a fairly smooth surface. Here five layers are exposed at a time.

(iii) The preparation $\wp(T_{\mathrm{G}} = 115$ K, $T_{\mathrm{A}} = 555$ K) results in an atomically smooth surface. Two layers are exposed only due to the fact that a noninteger number of MLs was evaporated onto the surface.

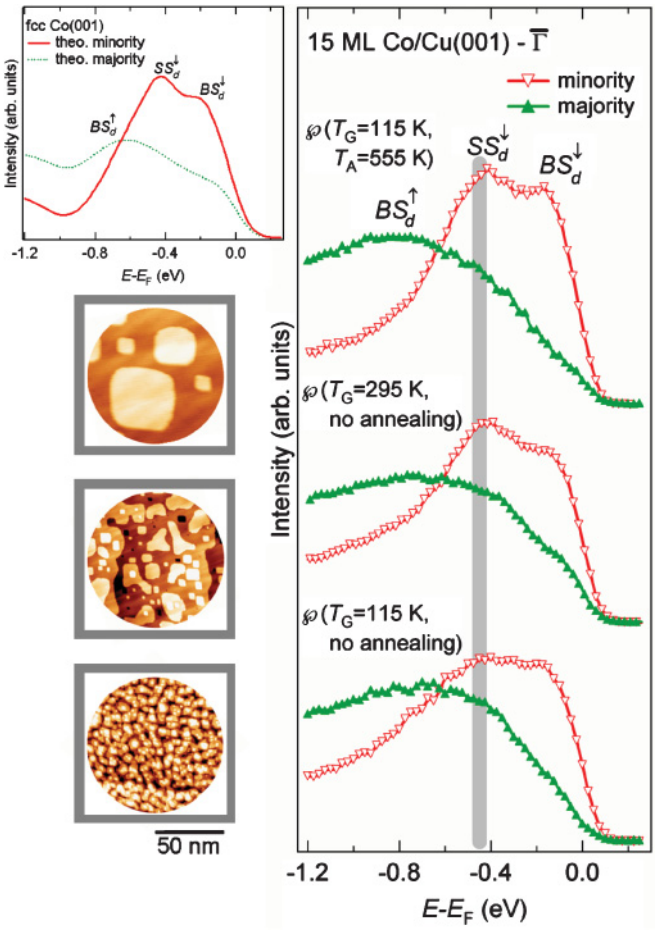

FIG. 1. (Color online) Spin-resolved PE measurements for 15-ML Co grown on Cu(001) for different growth and annealing temperatures (right-hand panel). The corresponding surface roughness is apparent in the STM measurements on the left-hand side. The PE measurements were obtained for normal electron emission at a sample temperature of $T = 145$ K. The spectra were normalized to equal background intensity at $E - E_{\mathrm{F}} = -4.1$ eV. The gray bar marks the position of the minority surface state $SS_d^{\downarrow}$. $BS_d^{\downarrow}$ and $BS_d^{\uparrow}$ are transitions from 3*d* bulk states with minority and majority-spin character, respectively. In addition, theoretical PE spectra for a Co(001) surface from a one-step model calculation are shown in the left upper corner of the figure.

The spectral feature of $SS_d^{\downarrow}$ is present in all spectra, yet with significantly different intensity. It directly reflects the degree of surface roughness: The smoother the surface, the higher is the intensity. For the atomically smooth surface, the spectral features appear even sharper than for the surface prepared at room temperature (RT). This is not only true for $SS_d^{\downarrow}$ but also for $BS_d^{\downarrow}$ (see detailed discussion below).

The experimental findings are in line with theoretical predictions, which expect a *d*-like occupied minority surface state at $\bar{\Gamma}$ at $E - E_{\mathrm{F}} = -0.45$ eV. The state $SS_d^{\downarrow}$ is located in a Δ_1-symmetry gap, which opens below $E - E_{\mathrm{F}} = -0.3$ eV for minority-spin electrons.[5] For majority-spin electrons, the symmetry gap opens below $E - E_{\mathrm{F}} = -1.6$ eV. The

majority-spin partner to $SS_d^{\downarrow}$ is, however, not observed in experiment nor does it appear in calculations, in which lifetime broadening effects of the initial states are taken into account. Lifetime broadening is mainly due to electron-hole pair decay, which is dominantly present in the majority spin channel.[12,13] If lifetime broadening effects are neglected in the calculation, the majority-spin partner $SS_d^{\uparrow}$ is located around $E - E_F = -1.7$ eV at the $\bar{\Gamma}$ point of the SBZ. Calculated spectra for Co(001) within the one-step formalism for photoemission are displayed in the left upper corner of Fig. 1, and resemble our experimental results.

In order to quantify the spectral width of the feature $SS_d^{\downarrow}$, we exposed the surfaces to 0.1 L ($1L = 1.3 \times 10^{-4}$ Pa s) of O_2 at $T = 145$ K. Figure 2 shows the spin-resolved data for the clean surface (dotted and solid lines) in comparison with the data for the surface exposed to O_2 (up- and downward pointing triangles) plus the difference spectra for minority spin (squares). The measurements were obtained for two different film preparations: $\wp(T_G = 115\ \text{K}, T_A = 555\ \text{K})$, and $\wp(T_G = 295\ \text{K}$, no annealing). The difference spectra

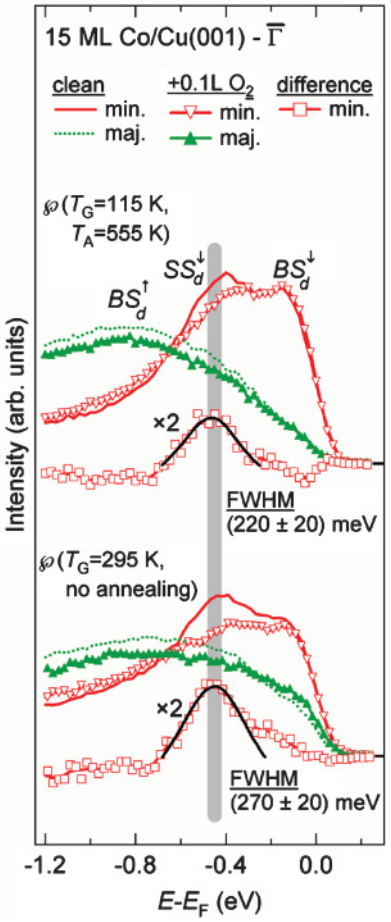

FIG. 2. (Color online) Spin-resolved PE measurements for two differently prepared 15-ML Co films on Cu(001) [$\wp(T_G = 115$ K, $T_A = 555$ K), $\wp(T_G = 295$ K, no annealing)] before and after exposure to oxygen. For each preparation, the spectra for the clean surface, for the surface exposed to 0.1 L of oxygen, and the difference spectrum for minority spin are shown. The difference spectra reveal the energy $E - E_F$ of $SS_d^{\downarrow}$ and its spectral width.

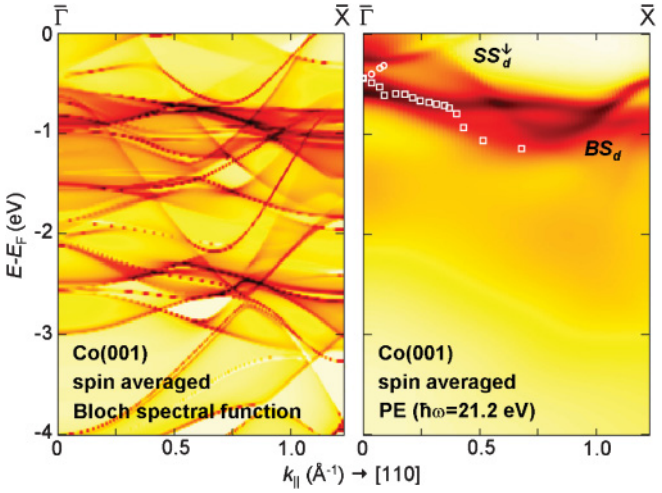

FIG. 3. (Color online) Color-coded contour plot for the calculated Bloch spectral function (left-hand side) and for the theoretical PE intensity obtained within the one-step model (right-hand side). High spectral intensity is indicated by dark colors. The dispersion of surface-related features, the minority surface state (labeled $SS_d^{\downarrow}$) and an additional surface-resonance-like state, was obtained by using the determinant criterion and is marked by circles and squares, respectively.

reveal the adsorbate-sensitive spectral features, i.e., primarily surface-related features. The width of $SS_d^{\downarrow}$ was estimated by fitting a Gaussian line to the surface-related feature around $E - E_F = -0.45$ eV. For the surface prepared at RT, the full width at half maximum (FWHM) of $SS_d^{\downarrow}$ amounts to (270 ± 20) meV whereas for the atomically smooth sample it is only (220 ± 20) meV. Here one should note that the absolute values depend on details of the background subtraction in the spectra for the clean and adsorbate-covered surface. Nevertheless, our analysis gives an indication toward a sharper surface state on the atomically smooth Co(001) surface. Our result is in line with the expectation that defects cause increased scattering[3] and scattering shortens the lifetime, which means an increase in linewidth.[1] Furthermore, this adsorbate experiment enabled us to verify the energy $E - E_F = -0.45$ eV for $SS_d^{\downarrow}$ at normal electron emission.

In addition to the calculated photoemission spectra for normal electron emission shown in Fig. 1, we calculated the Bloch spectral function for energies below the Fermi level as a function of $k_{\parallel}$ in the $\bar{\Gamma}\bar{X}$ direction (i.e., along ⟨110⟩). The results are shown in a color-coded contour plot in the left-hand panel of Fig. 3. High spectral intensity is indicated by dark colors. The calculation was done in a fully relativistic way, therefore the minority and majority-spin systems are not separated. The contour plot in the right-hand panel of Fig. 3 reflects the experimental situation. PE calculations using the one-step model take final-state and matrix element effects into account. Due to the pronounced lifetime broadening in the initial states, a strong smearing of all dipole-allowed spectral features appears for energies $E - E_F \leqslant -1.2$ eV.

The surface state $SS_d^{\downarrow}$ is clearly present at $E - E_F \approx -0.5$ eV at the $\bar{\Gamma}$ point. The dispersion of $SS_d^{\downarrow}$ around the $\bar{\Gamma}$ point is indicated by circles, which were determined by

employing the determinant criterium.[38] With increasing $k_\parallel$, the minority surface state disperses toward the Fermi level, crosses the Fermi level, and becomes unoccupied. The dispersion of the surface state is in line with experimental findings and previous slab calculations using density-functional theory in the local-density approximation by Miyamoto *et al.*[6] We note in passing that a second surfacelike feature is predicted by our determinant criterium and is marked by squares in the $E(k_\parallel)$ plot. This surface-resonance-like state shows the same dispersion as the Co 3*d* bulk bands. A surface-related state in this energy range was also predicted by slab calculations.[6]

B. Unoccupied exchange-split *sp*-like surface state

Face-centered-cubic crystals of noble and transition metals with (001) surface exhibit a characteristic unoccupied *sp*-like surface state within a gap of the surface-projected bulk-band structure. This gap is located mostly above the Fermi level, originates from a gap at the *L* high-symmetry point and appears around the $\bar{X}$ point of the SBZ.[7–9] Numerous IPE studies were dedicated to this state, e.g., on Cu,[39] Ag,[40] Ni,[41,42] Fe,[9,43] but the state was not observed for Co(001) so far. Figure 4 shows our spin-resolved IPE measurements of an atomically smooth fcc Co(001) surface for an electron incidence angle of

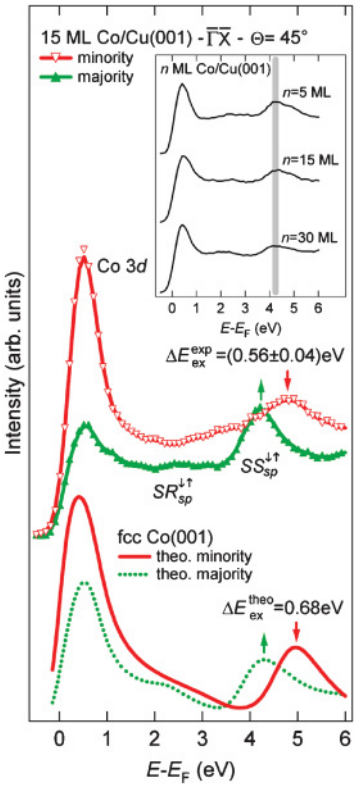

FIG. 4. (Color online) Spin-resolved IPE spectra for 15 MLs of Co on Cu(001) measured at room temperature for $\theta = 45^\circ$ along $\bar{\Gamma}\bar{X}$. The Co film was prepared at $T_G = 115$ K followed by an annealing to $T_A = 555$ K. The experimental data are shown in comparison with theoretical spectra for fcc Co(001). The inset shows spin-integrated IPE spectra for different film thicknesses: 5, 15, and 30 MLs. The surface state SS_{sp} (indicated by a gray bar) appears at the same energy for all thicknesses.

45° along the $\bar{\Gamma}\bar{X}$ direction (i.e., along ⟨110⟩) in comparison with a calculated spectrum. In the experiment, a spin-split spectral feature labeled $SS_{sp}^{\downarrow\uparrow}$ appears around 4.5 eV above the Fermi level. The minority-spin part of $SS_{sp}^{\downarrow\uparrow}$ is located at an energy of $E - E_F = (4.79 \pm 0.02)$ eV, the majority-spin part at $E - E_F = (4.23 \pm 0.02)$ eV (see the thin vertical arrows in Fig. 4). At the electron incidence angle of 45°, $SS_{sp}^{\downarrow\uparrow}$ is probed close to the $\bar{X}$ point of the SBZ, where the band minimum is expected. Thus the experimentally observed spin splitting resembles the exchange splitting and amounts to $\Delta E_{ex}^{exp} = (0.56 \pm 0.04)$ eV. This corresponds to the theoretical result: $\Delta E_{ex}^{theo} = 0.68$ eV. Here, the minority surface state $SS_{sp}^{\downarrow}$ is located at $E - E_F = 4.98$ eV and the majority-spin partner at $E - E_F = 4.30$ eV.

Two further spectral features are observed in Fig. 4: (i) A spin-split feature labeled $SR_{sp}^{\downarrow\uparrow}$ between 2 and 3 eV above E_F with pronounced majority but only weak minority intensity in experiment and theory. From the theoretical calculations using the determinant criterium, surface character is attributed to $SR_{sp}^{\downarrow\uparrow}$. It appears along the boundary of a gap in the projected bulk-band structure and is found as a surface resonance also on the equivalent surfaces of Cu,[37] Ni,[42] and Fe.[9,43] (ii) The pronounced intensity with predominant minority character close to E_F originates from Co 3*d* bulk bands. Empty minority *d* states plus an *sp* band crossing E_F with increasing angle of electron incidence are responsible for the observed intensities. The majority intensity is less pronounced for normal electron incidence (not shown here).

We can exclude that the feature $SS_{sp}^{\downarrow\uparrow}$ in our data for 15-ML-thick films stems from quantum-well states (QWSs) for two reasons: (i) In a former study, *sp*-type QWSs were identified for film thicknesses of up to 10 MLs.[44] Already at a thickness of 12 MLs, bulklike transitions were observed. (ii) As shown in the inset of Fig. 4, the energetic position of the state SS_{sp} (indicated by a gray bar) does not depend on the film thickness, whereas QWS energies depend strongly on the film thickness. Moreover, the state SS_{sp} is highly sensitive toward oxygen exposure (not shown), which is a characteristic behavior of surface states.

To investigate the sensitivity of $SS_{sp}^{\downarrow\uparrow}$ to surface roughness, we performed spin-integrated IPE measurements for varied surface preparations resulting in different surface topographies. Our results are displayed in Fig. 5 for four different surface preparations (from bottom to top):

(i) Preparation $\wp(T_G = 115$ K, no annealing).

(ii) Preparation $\wp(T_G = 115$ K, $T_A = 295$ K). The annealing to $T_A = 295$ K results in an increased Co adatom mobility, which allows the Co to arrange in larger rectangular islands. This reduces the film roughness in comparison to $\wp(T_G = 115$ K, no annealing).

(iii) Preparation $\wp(T_G = 295$ K, no annealing).

(iv) Preparation $\wp(T_G = 115$ K, $T_A = 555$ K).

For low-temperature film growth without annealing, the surface is roughest and no surface state is observed. The spectral intensity of SS_{sp} increases with decreasing surface roughness. When the sample is annealed to RT ($\wp(T_G = 115$ K, $T_A = 295$ K)), the island size increases and, as a consequence, the roughness decreases. For a Co film grown at

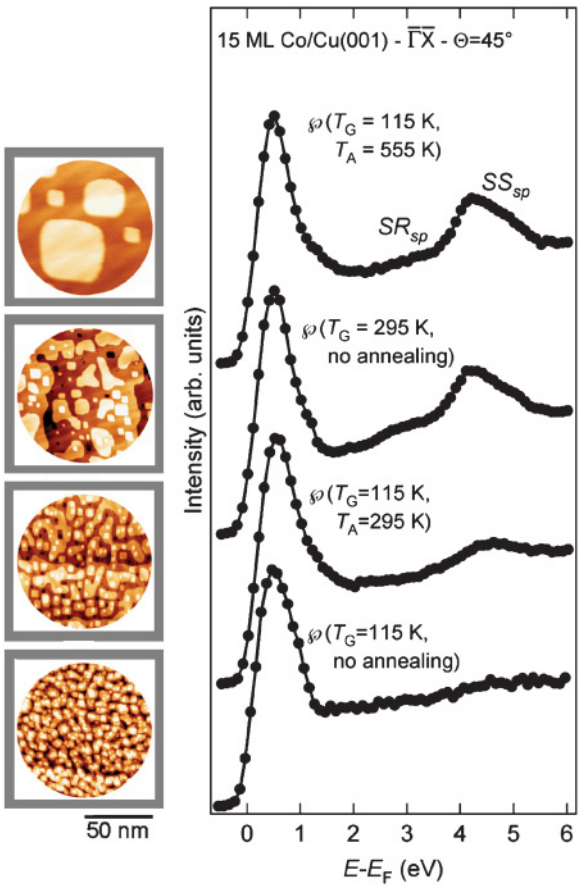

FIG. 5. (Color online) Spin-integrated IPE measurements of 15-ML Co grown on Cu(001) for different surface topographies (right-hand side) in relation to corresponding STM measurements (left-hand side). For the preparations $\wp(T_G = 115\ K, T_A = 555\ K)$ and $\wp(T_G = 115\ K, T_A = 295\ K)$, the sample temperature was $T = 295$ K during the measurement. For the preparations $\wp(T_G = 295\ K$, no annealing) and $\wp(T_G = 115\ K$, no annealing) the sample temperature was $T = 145$ K during the measurement. The spectra were normalized to equal background intensity.

RT [$\wp(T_G = 295\ K$, no annealing)] the surface-state intensity is about as high as for an atomically smooth film [$\wp(T_G = 115\ K, T_A = 555\ K)$].

In contrast to the occupied d-like minority surface state, which is present independent of the preparation conditions, yet with different intensity, the unoccupied sp-like spin-split surface state is absent for the film with highest roughness. Its intensity increases significantly as soon as the Co islands at the surface get larger and the roughness decreases. This behavior is a consequence of the different lateral extensions of the respective wave functions, more localized for d and less localized for sp states.

Finally, we present fully relativistic LSDA+DMFT Bloch spectral function and corresponding one-step model calculations for the unoccupied electronic structure. The results are shown in a color-coded contour plot in Fig. 6. The left-hand panel shows the Bloch spectral function for the unoccupied states along $\bar{\Gamma}\bar{X}$. Several spectral features can be distinguished, in particular the spin-split surface state $SS_{sp}^{\downarrow\uparrow}$ around $\bar{X}$ at an energy of $E - E_F = 4.98$ eV for $SS_{sp}^{\downarrow}$ and at $E - E_F =$ 4.30 eV for $SS_{sp}^{\uparrow}$. The right-hand panel of Fig. 6 shows one-step-model IPE calculations for $\hbar\omega = 9.9$ eV. Compared with the Bloch spectral function, the IPE contour plot contains the spin-split surface state $SS_{sp}^{\downarrow\uparrow}$ only as a weak intensity smeared out in energy because of strong damping effects, which are neglected in the calculation of the Bloch spectral function. On the other hand, the series of image-potential states $IS^{\downarrow\uparrow}$ is not reproduced by the Bloch spectral function. They only show up in calculations with realistic Coulomb-like surface potential, which is not included in the LSDA approach using an exponential decay instead. The spin-split sp-like surface resonance $SR_{sp}^{\downarrow\uparrow}$ in Fig. 4 is hardly visible as a dispersing feature in the IPE calculations because of its overlap with bulk states and due to damping effects, which are more pronounced for higher energies. To determine the dispersion behavior of $SR_{sp}^{\downarrow\uparrow}$, we performed an additional calculation, in which we neglected broadening effects and included impurity scattering only by a small constant imaginary value of $iV_i = 0.05$ eV. The derived spin-resolved dispersion is shown in Fig. 6(b) as green up and red down triangles.

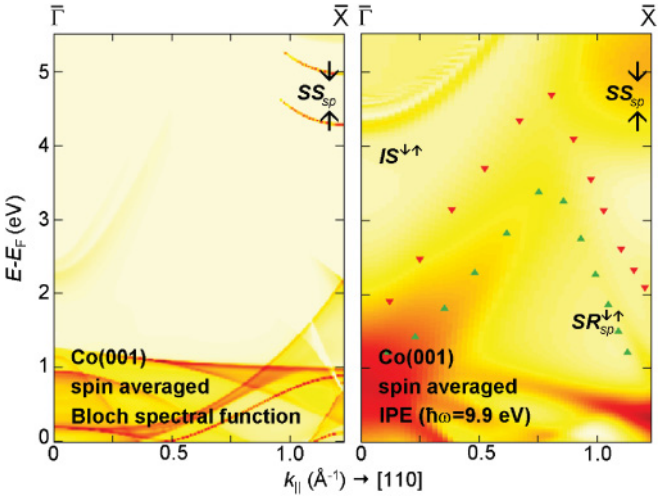

FIG. 6. (Color online) Color-coded contour plot for the calculated Bloch spectral function of the unoccupied electronic structure of Co(001) (left-hand side). Calculations within the one-step model of IPE for $\hbar\omega = 9.9$ eV (right-hand side). High spectral intensity is indicated by dark colors. The dispersion behavior of the sp-like surface resonance $SR_{sp}^{\downarrow\uparrow}$ is indicated by green up and red down triangles for the majority and minority-spin channels, respectively.

IV. SUMMARY

We identified two crystal-induced surface states for fcc Co(001), experimentally realized by a 15-ML-thick Co film on Cu(001). A d-like occupied surface state of minority-spin character labeled $SS_d^{\downarrow}$ appears 0.45 eV below the Fermi energy around the $\bar{\Gamma}$ point of the surface Brillouin zone. A sp-like unoccupied surface state labeled $SS_{sp}^{\downarrow\uparrow}$ appearing at about 4.5 eV above the Fermi level at the zone boundary $\bar{X}$ is found to be exchange split by 0.56 eV. Both surface states are well described by fully relativistic LSDA+DMFT calculations of the Bloch spectral function and corresponding one-step model calculations of the spectral intensities. The good agreement

between experiment and theory concerning the dispersion behavior of the occupied surface resonance is due to the real part of the self energy. This quantity causes a shift of the various d bands located in the vicinity of the Fermi level of about 0.2 eV toward E_F.

The two different surface states show a distinct sensitivity to surface roughness. The spectral intensities for both states are most pronounced on the atomically smooth surface, where, in addition, the spectral width of $SS_d^{\downarrow}$ is smallest. However, the two states respond differently to lateral inhomogeneities. While the d-like surface state $SS_d^{\downarrow}$ is not quenched by surface roughness, $SS_{sp}^{\downarrow\uparrow}$ does not appear on the rough surface with island sizes between 3 and 6 nm. These observations can be understood as a consequence of the different types of wave functions. The more localized d-like wave function is less sensitive to lateral inhomogeneities than the less localized sp-type wave function.

ACKNOWLEDGMENTS

It is a pleasure to thank Ch. Eibl and V. Renken for helpful discussions and W. Mai and H. Wensing for technical support. This work was supported by the Deutsche Forschungsgemeinschaft (Grants No. EBE - 154/18 and No. FOR1346) and the Bundesministerium für Bildung und Forschung (Grants No. 05KI0WW1/2 and No. 05KSIWMB/1).

*tobias.allmers@uni-muenster.de
†markus.donath@uni-muenster.de

[1] F. Theilmann, R. Matzdorf, and A. Goldmann, Surf. Sci. **420**, 33 (1999).
[2] K. Boger, M. Weinelt, and Th. Fauster, Phys. Rev. Lett. **92**, 126803 (2004).
[3] G. Jnawali, Th. Wagner, H. Hattab, R. Möller, A. Lorke, and M. Horn-von Hoegen, e-J. Surf. Sci. Nanotech. **8**, 27 (2010).
[4] T. Allmers and M. Donath, Surf. Sci. **605**, 1875 (2011).
[5] A. B. Schmidt, M. Pickel, T. Allmers, M. Budke, J. Braun, M. Weinelt, and M. Donath, J. Phys. D **41**, 164003 (2008).
[6] K. Miyamoto, K. Iori, K. Sakamoto, H. Narita, A. Kimura, M. Taniguchi, S. Qiao, K. Hasegawa, K. Shimada, H. Namatame, and S. Blügel, New J. Phys. **10**, 125032 (2008).
[7] A. Goldmann, V. Dose, and G. Borstel, Phys. Rev. B **32**, 1971 (1985).
[8] N. V. Smith, C. T. Chen, and M. Weinert, Phys. Rev. B **40**, 7565 (1989).
[9] M. Donath, M. Pickel, A. B. Schmidt, and M. Weinelt, J. Phys.: Condens. Matter **21**, 134004 (2009).
[10] J. Braun, J. Minár, H. Ebert, M. I. Katsnelson, and A. I. Lichtenstein, Phys. Rev. Lett. **97**, 227601 (2006).
[11] M. Pickel, A. B. Schmidt, F. Giesen, J. Braun, J. Minár, H. Ebert, M. Donath, and M. Weinelt, Phys. Rev. Lett. **101**, 066402 (2008).
[12] J. Sanchez-Barriga, J. Fink, V. Boni, I. Di Marco, J. Braun, J. Minár, A. Varykhalov, O. Rader, V. Bellini, F. Manghi, H. Ebert, M. I. Katsnelson, A. I. Lichtenstein, O. Eriksson, W. Eberhardt, and H. A. Dürr, Phys. Rev. Lett. **103**, 267203 (2009).
[13] J. Sanchez-Barriga, J. Minár, J. Braun, A. Varykhalov, V. Boni, I. Di Marco, O. Rader, V. Bellini, F. Manghi, H. Ebert, M. I. Katsnelson, A. I. Lichtenstein, O. Eriksson, W. Eberhardt, H. A. Dürr, and J. Fink, Phys. Rev. B **82**, 104414 (2010).
[14] G. Kotliar and D. Vollhardt, Phys. Today **57**(3), 53 (2004).
[15] A. Georges, G. Kotliar, W. Krauth, and M. J. Rozenberg, Rev. Mod. Phys. **68**, 13 (1996).
[16] G. Malmström and J. Rundgren, Comput. Phys. Commun. **19**, 263 (1980).
[17] C. M. Schneider, P. Bressler, P. Schuster, J. Kirschner, J. J. de Miguel, and R. Miranda, Phys. Rev. Lett. **64**, 1059 (1990).
[18] M. Budke, T. Allmers, M. Donath, and G. Rangelov, Rev. Sci. Instrum. **78**, 113909 (2007).
[19] J. Kirschner and R. Feder, Phys. Rev. Lett. **42**, 1008 (1979).
[20] D. H. Yu, C. Math, M. Meier, M. Escher, G. Rangelov, and M. Donath, Surf. Sci. **601**, 5803 (2007).
[21] M. Donath, Surf. Sci. Rep. **20**, 251 (1994).
[22] M. Budke, V. Renken, H. Liebl, G. Rangelov, and M. Donath, Rev. Sci. Instrum. **78**, 083903 (2007).
[23] D. Funnemann and H. Merz, J. Phys. E **19**, 544 (1986).
[24] S. van Dijken, G. Di Santo, and B. Poelsema, Phys. Rev. B **63**, 104431 (2001).
[25] S. H. Vosko, L. Wilk, and M. Nusair, Can. J. Phys. **58**, 1200 (1980).
[26] H. Ebert and B. L. Gyorffy, J. Phys. F **18**, 451 (1988).
[27] H. Ebert, in *Electronic Structure and Physical Properties of Solids*, Lecture Notes in Physics No. 535, edited by H. Dreyssé (Springer, Berlin, 2000), p. 191.
[28] P. Hohenberg and W. Kohn, Phys. Rev. **136**, B864 (1964); W. Kohn and L. J. Sham, *ibid.* **140**, A1133 (1965); L. J. Sham and W. Kohn, *ibid.* **145**, 561 (1966).
[29] R. O. Jones and O. Gunnarsson, Rev. Mod. Phys. **61**, 689 (1989).
[30] J. Minár, L. Chioncel, A. Perlov, H. Ebert, M. I. Katsnelson, and A. I. Lichtenstein, Phys. Rev. B **72**, 045125 (2005).
[31] M. I. Katsnelson and A. I. Lichtenstein, Eur. Phys. J. B **30**, 9 (2002).
[32] L. V. Pourovskii, M. I. Katsnelson, and A. I. Lichtenstein, Phys. Rev. B **72**, 115106 (2005).
[33] V. I. Anisimov and O. Gunnarsson, Phys. Rev. B **43**, 7570 (1991).
[34] V. I. Anisimov, F. Aryasetiawan, and A. I. Lichtenstein, J. Phys.: Condens. Matter **9**, 767 (1997).
[35] W. Wallauer and T. Fauster, Phys. Rev. B **54**, 5086 (1996).
[36] S. Hüfner, *Photoelectron Spectroscopy: Principles and Applications*, 3rd ed. (Springer, Berlin Heidelberg, 2003).
[37] M. Graß, J. Braun, G. Borstel, R. Schneider, H. Dürr, Th. Fauster, and V. Dose, J. Phys.: Condens. Matter **5**, 599 (1993).
[38] J. Braun and M. Donath, J. Phys.: Condens. Matter **16**, 2539 (2004).
[39] V. Dose, U. Kolac, G. Borstel, and G. Thörner, Phys. Rev. B **29**, 7030 (1984).
[40] B. Reihl, K. H. Frank, and R. R. Schlittler, Phys. Rev. B **30**, 7328 (1984).
[41] K. Starke, K. Ertl, and V. Dose, Phys. Rev. B **45**, 6154 (1992).
[42] R. Schneider, K. Starke, K. Ertl, M. Donath, V. Dose, J. Braun, M. Grass, and G. Borstel, J. Phys.: Condens. Matter **4**, 4293 (1992).
[43] B. Gubanka, M. Donath, and F. Passek, J. Magn. Magn. Mater. **161**, L11 (1996).
[44] D. H. Yu, M. Donath, J. Braun, and G. Rangelov, Phys. Rev. B **68**, 155415 (2003).